Article

Enhancing the Photocatalytic Degradation of Methylene Blue with Graphene Oxide-Encapsulated g-C$_3$N$_4$/ZnO Ternary Composites

Muhammad Hassan Shakoor, Muhammad Bilal Shakoor,* Asim Jilani, Toheed Ahmed, Muhammad Rizwan, Mohsin Raza Dustgeer, Javed Iqbal, Muhammad Zahid, and Jean Wan Hong Yong*

Read Online

ACCESS | Metrics & More | Article Recommendations | Supporting Information

ABSTRACT: Methylene blue (MB) is a toxic contaminant present in wastewater. Here, we prepared various composites of graphene oxide (GO) with graphitic carbon nitride (g-C$_3$N$_4$) and zinc oxide (ZnO) for the degradation of MB. In comparison to ZnO (22.9%) and g-C$_3$N$_4$/ZnO (76.0%), the ternary composites of GO/g-C$_3$N$_4$/ZnO showed 90% photocatalytic degradation of MB under a light source after 60 min. The experimental setup and parameters were varied to examine the process and effectiveness of MB degradation. Based on the results of the experiments, a proposed photocatalytic degradation process that explains the roles of GO, ZnO, and g-C$_3$N$_4$ in improving the photocatalytic efficacy of newly prepared

GO/g-C$_3$N$_4$/ZnO was explored. Notably, the g-C$_3$N$_4$/ZnO nanocomposite's surface was uniformly covered with ZnO nanorods. The images of the samples clearly demonstrated the porous nature of GO/g-C$_3$N$_4$/ZnO photocatalysts, and even after being mixed with GO, the g-C$_3$N$_4$/ZnO composite retained the layered structure of the original material. The catalyst's porous structure plausibly enhanced the degradation of the contaminants. The high-clarity production of g-C$_3$N$_4$ and the effectiveness of the synthesis protocol were later validated by the absence of any trace contamination in the energy-dispersive X-ray spectroscopy (EDS) results. The composition of the ZnO elements and their spectra were revealed by the EDS results of the prepared ZnO nanorods, g-C$_3$N$_4$/ZnO, and GO/g-C$_3$N$_4$/ZnO. The outcomes indicated that the nanocomposites were highly uncontaminated and contained all necessary elements to facilitate the transformative process. The results of this experiment could be applied at a large scale, thus proving the effectiveness of photocatalysts for the removal of dyes.
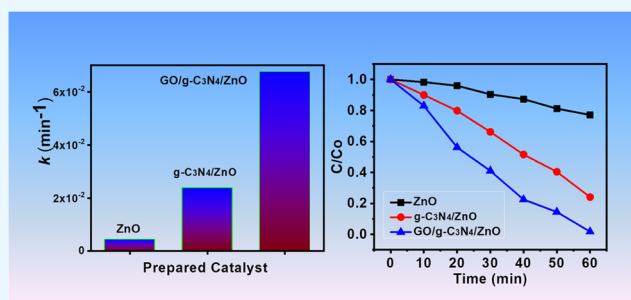
1. INTRODUCTION

Water pollution is the contamination of natural water resources, such as lakes, rivers, oceans, and groundwater, with substances that are hazardous to living organisms and the ecosystems. Methylene blue (MB) is an aromatic compound having a heterocyclic structure. It is frequently used dye in paper and textile, wool, and silk industry.[1] If ingested or comes into direct contact with the skin surface, MB is extremely dangerous. The discharge of partially or untreated MB dye-loaded wastewater from any industrial production may pose a number of health risks.[2] In humans, for example, MB dye can cause jaundice, cyanosis, tissue necrosis, vomiting, higher heart rate, and cancers of different types.[3] Furthermore, the existence of MB has evolved into a massive issue for plants, causing growth inhibition, pigment minimization, and a reduction in the microalgae protein content. As a matter of fact, before releasing MB-polluted wastewater into freshwater environments, this poisonous dye should be removed.[4]

Contamination from water can be reduced using the energy of light via a process called photocatalysis. A photocatalyst is a substance that can absorb light energy and utilize it to stimulate chemical reactions which is the main part of this

process.[5] One benefit of treatment of wastewater by photocatalysis is that a variety of pollutants, including those that are challenging to remove by other methods, can be broken down using this approach.[6,7] The quantity of impurities released into the surroundings can be minimized by using treatment of wastewater by photocatalysis, which can be more effective and affordable than conventional chemical treatment approaches.[8] The photocatalytic process can be applied in a variety of methods; for example, employing a photocatalytic reactor, which is an enclosed area where water is exposed to light while being in the presence of a photocatalyst, is one favored technique. Additionally, it can be used to detoxify water by destroying microorganisms.[9,10] Materials containing at least a single dimension in the nanoscale range are called nanomaterials (typically between 1 and 100 nm).[11] These substances
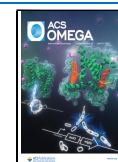
have unique characteristics that make them beneficial for treating wastewater.[12,13] Graphene and carbon nanotubes are two main examples of nanoparticles containing a high surface area-to-volume ratio. These substances are easily eliminated from water for disposal and have a significant capacity for adsorbing contaminants. Another technique for disinfecting wastewater with nanomaterials is facilitated by harnessing the catalytic processes, which is the stimulation of several chemical reactions.[14] Metallic nanoparticles like silver and gold can stimulate the degradation of wastewater pollutants like microorganisms and organic substances.[15] Additionally, photocatalysis,[16] as we previously discussed, is a different method of water purification that may be applied by using semiconductor nanoparticles, including silicone dioxide, titanium dioxide, and zinc oxide as a photocatalyst, which is more effective and demands fewer doses of ultraviolet light. Overall, introducing nanomaterials to water treatment shows potential for raising the effectiveness and efficiency of existing wastewater treatment systems.[17,18] Before bringing these materials on a commercial scale, it is crucial to carefully assess the potential effects they may have on human health and the environment and put safety precautions in position. Zinc oxide (ZnO) is a semiconductor substance that has been investigated as a photocatalyst for the decontamination of wastewater.[19] As a photocatalyst, ZnO has several benefits, including its wide range of band gap, which enables it to absorb an extensive range of wavelengths of light, and its relatively low toxicity. Zinc oxide produces hole pairs of electrons when subjected to light, which can then be used to oxidize contaminants in water.[20] It has been discovered that ZnO is good in oxidizing a variety of contaminants, including organic materials, microorganisms, and pathogens. Additionally, the performance of ZnO is improved by preparing ZnO nanoparticles having enlarged surface area-to-volume ratio thus improving the active sites for photocatalytic degradation of pollutants.[21] The ZnO can also be combined with various metallic nanoparticles, which could act as cocatalysts and enhance the activity of ZnO in photocatalysis.[22] It is important to keep in mind that ZnO has several limitations, including the fact that photocatalytic activity is only limited to visible light, which means that UV light is the main activator for the photocatalytic process. Furthermore, it has been discovered that ZnO is less persistent in acidic and basic conditions, which may restrict its application in particular wastewater treatment scenarios.[23] However, due to its wide range of band gap, low degree of toxicity, and adaptability in a variety of applications, ZnO is a potential photocatalyst for wastewater treatment; nevertheless, more research is required to improve its performance and overcome its drawbacks.[24]

The graphitic carbon nitride (g-C$_3$N$_4$) is used to purify wastewater through an approach called photocatalytic oxidation, which uses the energy of light to degrade contaminants in water. Reactive oxygen species, such as hydroxyl radicals, can be produced using g-C$_3$N$_4$ and subsequently can be used to degrade harmful substances in water. Making g-C$_3$N$_4$-based composite materials is yet another method where g-C$_3$N$_4$ is used to remediate water.[25] To increase the photocatalytic activity of g-C$_3$N$_4$, researchers have been investigating ways of merging it with other substances, such as metal nanoparticles, which may operate as cocatalysts.[26] It was known that the g-C$_3$N$_4$ is effective at degrading different contaminants and volatile organic compounds in other applications, through a process of air

filtration.[27] Nevertheless, more research pertaining to g-C$_3$N$_4$ is needed before it can be used extensively in water treatment systems. For example, new study is required to improve the synthesis of g-C$_3$N$_4$ and to produce it at a lower cost on a larger scale. To facilitate large-scale implementation and with human health consideration, new research is required to evaluate the enduring stability and safety hazards of g-C$_3$N$_4$ in applications involving water treatment. As a powerful photocatalyst for wastewater treatment, g-C$_3$N$_4$ has a wide range of uses and was proven to be highly effective at removing contaminants under laboratory conditions.[28]

Graphene is considered an important 2D material for different applications such as heterogeneous catalysis, adsorption, and photocatalysis owing to its promising characteristics including outstanding thermal conductivity, higher mechanical strength, and electron mobility.[29,30] Graphene is a highly efficient photocatalytic material due to its high surface area providing a suitable support for ZnO nanoparticles and thus improving the photocatalytic degradation of pollutants.[31,32] Graphene oxide (GO) is a promising material for water treatment with high adsorption capacity, catalytic activity, and mechanical stability. But its scalability, cost-effectiveness, and safety require further assessment and consideration.[33] Therefore, herein, we prepared a combination of ZnO with GO and g-C$_3$N$_4$ using the wet impregnation method. The role of GO and g-C$_3$N$_4$ in improving the photocatalytic performance of ZnO was assessed. Furthermore, the variations in surface functional groups using the XPS technique and changes in the optical and structural features of prepared nanocomposites were also determined.

2. MATERIAL AND METHODS

2.1. Materials. Analytical grade sulfuric acid (H$_2$SO$_4$) (95−98%), graphite (99%), hydrogen peroxide (H$_2$O$_2$) (37%), and phosphoric acid (H$_3$PO$_4$) (85%) were bought from Sigma-Aldrich company. Zinc acetate dihydrate (99.99%) and potassium permanganate (KMnO$_4$) (97%) were obtained from Merck and Alfa Aesar, respectively. Methylene blue (95%), melamine (99%), and graphite flakes were bought from the internationally reputable chemical company (Sigma-Aldrich) and used in the tests without further processing.

2.2. Preparation of Graphene oxide. The most common and widely used method is Hummer's method for making graphene oxide. Graphene oxide (GO) is also sometimes called graphitic acid. For graphene oxide preparation, 3 g of graphite and 18 g of KMnO$_4$ with a 9:1 ratio of H$_2$SO$_4$ to H$_3$PO$_4$ was mixed and the final volume was made up to 400 mL. After 12 h of continuous stirring at a temperature of 50 °C, the reaction mixture was poured into 400 mL of ice by making an ice bath. After the mixture was cooled while being continuously stirred by a glass rod, it was treated with H$_2$O$_2$ having a quantity of 3 mL for precipitated GO. The mixture of GO was washed with hydrochloric acid (HCl) (5%), deionized water, and ethanol before filtration. Finally, GO solution was obtained and centrifuged for additional purification and graphene oxide sheets preparation.[34]

2.3. Preparation of Zinc Oxide. Zinc oxide (ZnO) nanoparticles were prepared by direct heating. Zinc acetate was used as a precursor to create ZnO photocatalyst. 50 mL of ethanol was combined with 3 g of zinc acetate dihydrate and vigorously stirred. The material was shifted to an aluminum crucible after 2 h of continuous stirring, where it was heated for 60 min at 400 °C in a muffle furnace to convert it into ZnO.
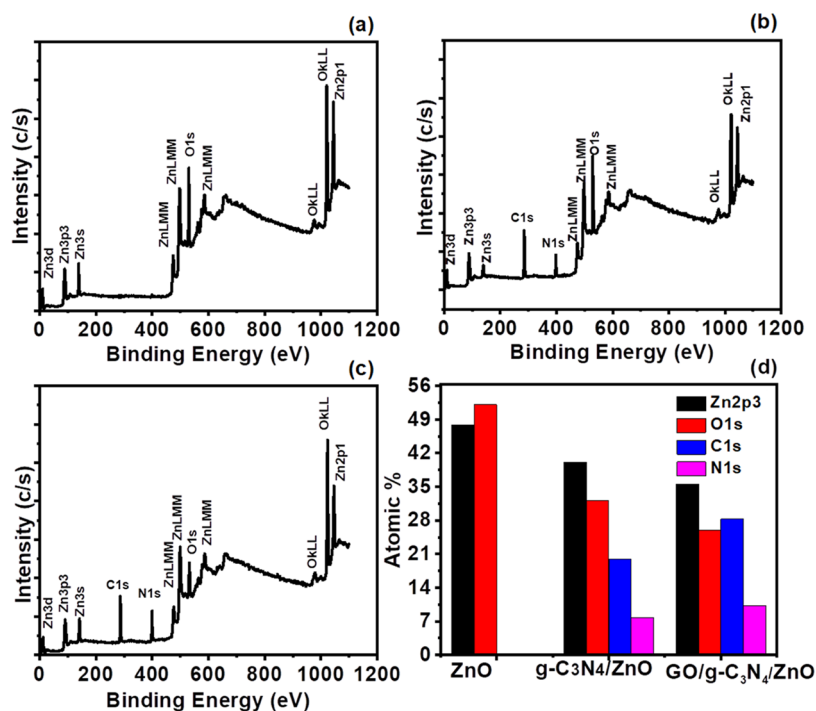
Figure 1. XPS spectra of ZnO (a), g-C_3N_4/ZnO (b), and GO/g-C_3N_4/ZnO (c) and atomic percentage of ZnO, g-C_3N_4/ZnO, and GO/g-C_3N_4/ZnO (d).
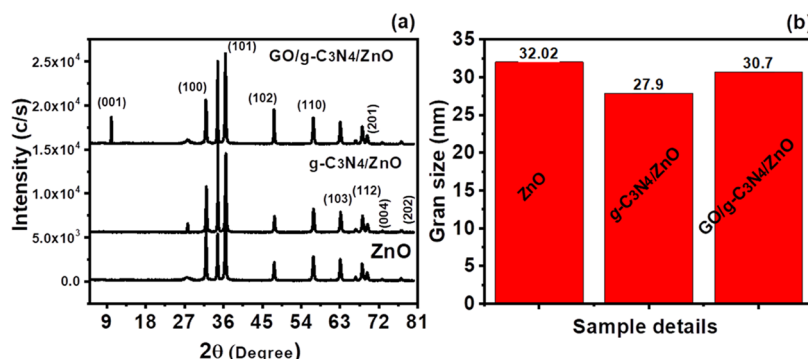

Figure 2. (a) Diffraction patterns of ZnO, g-C_3N_4/ZnO, and GO/g-C_3N_4/ZnO. (b) Grain size of ZnO, g-C_3N_4/ZnO, and GO/g-C_3N_4/ZnO.

Finally, we obtained the ZnO nanoparticles which were converted into a powdered form.[35]

2.4. Preparation of Graphitic Carbon Nitride (g-C_3N_4). 5 g of melamine was weighed at room temperature, covered with a ceramic crucible, and then placed in a muffle furnace for heating. The temperature of heating was increased at 20 °C/min and continued for 2 h. The final temperature achieved was 550 °C. The sample was kept for heating in a furnace for 5 h. After heating, the crucible was cooled and the sample was converted into a powdered form.[36]

2.5. Synthesis of GO/g-C_3N_4/ZnO. The GO/g-C_3N_4/ZnO was prepared by a wet impregnation method. This method was beneficial for the synthesis of GO/g-C_3N_4/ZnO due to its simplicity and low synthesizing cost for photocatalytic degradation. 2% weight of graphene oxide, 38% weight of g-C_3N_4, and 60% weight of ZnO were combined in ethanol solution. The mixture was continuously stirred for 120 min. The centrifuge technique was used to separate the ethanol from the mixture at 3500 rpm. The obtained mixture was dried in an oven for 120 min to get the final product of GO/g-C_3N_4/ZnO.[37]

2.6. Characterization of GO/g-C_3N_4/ZnO. The GO/g-C_3N_4/ZnO structure was examined using a Rigaku Ultima IV X-ray diffraction (XRD). Versa PobeII X-ray photoelectron spectroscopy (XPS) was used to investigate the surface characteristics and chemical composition. Surface morphology was examined using a scanning electron microscope (JEOL, JSM7600-F). The absorption spectra for the degradation of methylene blue (MB) were obtained through a spectrophotometer (DR 6000, Hach Lang).

2.7. Photocatalytic Degradation Test. In order to test the photocatalytic abilities of GO/g-C_3N_4/ZnO, 20 mg of the catalysts was added to 200 mL of 15 ppm of MB. To achieve absorption equilibrium, the solution was continuously stirred while being kept in the dark for 1 h. The solution was then exposed to visible light (100 W) for the following 60 min, with 2 mL being taken every 10 min for deterioration analysis.[38] The degradation percentage and reaction rate constant were determined using the formulas below (eqs 1 and 2):

$$\text{degradation (\%)} = \left(\frac{C_0 - C_t}{C_0} \right) \times 100 \tag{1}$$

$$\ln \left(\frac{C}{C_0} \right) = -kt \tag{2}$$

3. RESULTS AND DISCUSSION

3.1. Surface Compositional Analysis. The O1s spectra of zinc oxide (ZnO) (Figure 1a) demonstrated the presence of only one peak at around 530 eV which was attributed to the presence of Zn−O having 50% atomic ratio. However, C 1s spectra were present in g-C$_3$N$_4$/ZnO as well as the N1s and O1s peaks were also observed at 290, 400, and 540 eV.[39] These spectra showed that their atomic ratios are 20, 8, and 33% respectively. After adding graphitic carbon nitride (g-C$_3$N$_4$) to ZnO, a small shift was observed in O1s spectra as compared to ZnO only. The atomic percentage of C=O=C decreased from 50 to 33%.[40] The C1s, N1s, and O1s spectra in GO/g-C$_3$N$_4$/ZnO comparatively also observed around the peaks of 290, 400, and 540 eV, which are attributed to the atomic ratios of related elements, that is, 26, 10, and 24%, respectively.[40]

The Zn2p3 spectrum of GO/g-C$_3$N$_4$/ZnO (depicted in Figure S1a) exhibits three discernible peaks at approximately 1019, 1022, and 1025 eV. The peak at 1019 eV is ascribed to Zn^{2+}, while the peaks at 1022 and 1025 eV are indicative of zinc interacting with oxygen (Zn−O) and hydroxyl groups, respectively.[41] Analyzing the O1s spectra of ZnO (as shown in Figure S1b) reveals three distinctive peaks at approximately 529, 531, and 533 eV, corresponding to metal interaction (O metal), oxygen vacancies (O$_V$), and hydroxyl interaction (OH), respectively.[41] The existence of oxygen vacancies and hydroxyl interactions creates binding sites that facilitate the capture of dye molecules, effectively reducing the charge recombination ratio. This phenomenon contributes to the augmented photocatalytic degradation of ZnO-based composites.[42]

3.2. XRD. X-ray diffraction (XRD) analysis was employed to investigate the structural properties and crystallinity of pristine g-C$_3$N$_4$ and ZnO, as well as their composite materials (GO/g-C$_3$N$_4$/ZnO). The spectra of ZnO revealed a prominent peak at 2θ = 36.40°, which was attributed to the diffraction plane (101) (Figure 2). Additionally, there were less intense peaks observed at 2θ = 32.02, 34.73, 48.50, 55.75, 63.09, 66.50, 68.80, 69.30, and 72.70°, attributed to planes (100), (001), (102), (110), (103), (201), (200), (112), and (004), respectively. The ZnO diffraction pattern alignment with the JCPD 01-073-6865 card indicated that ZnO nanorods possessed a zincite structure. In g-C$_3$N$_4$/ZnO, the XRD spectrum showed that distinct ZnO peaks were observed, in conjunction with a weak g-C$_3$N$_4$ peak (Figure 2a). The ternary composite (GO/g-C$_3$N$_4$/ZnO) exhibited identical peak patterns of diffraction. However, the GO component did not exhibit sharp peaks; instead, it displayed a little dip which was overshadowed due to the occurrence of strong peaks. Nevertheless, a weak g-C$_3$N$_4$ peak was discernible in the spectrum of ternary nanocomposite, the same as observed in g-C$_3$N$_4$/ZnO composites (Figure 2a).[37] The existence of ZnO and g-C$_3$N$_4$/ZnO diffraction peak patterns in the prepared nanocomposites confirmed the preparation of ternary composites, which exhibited crystalline properties. The mean
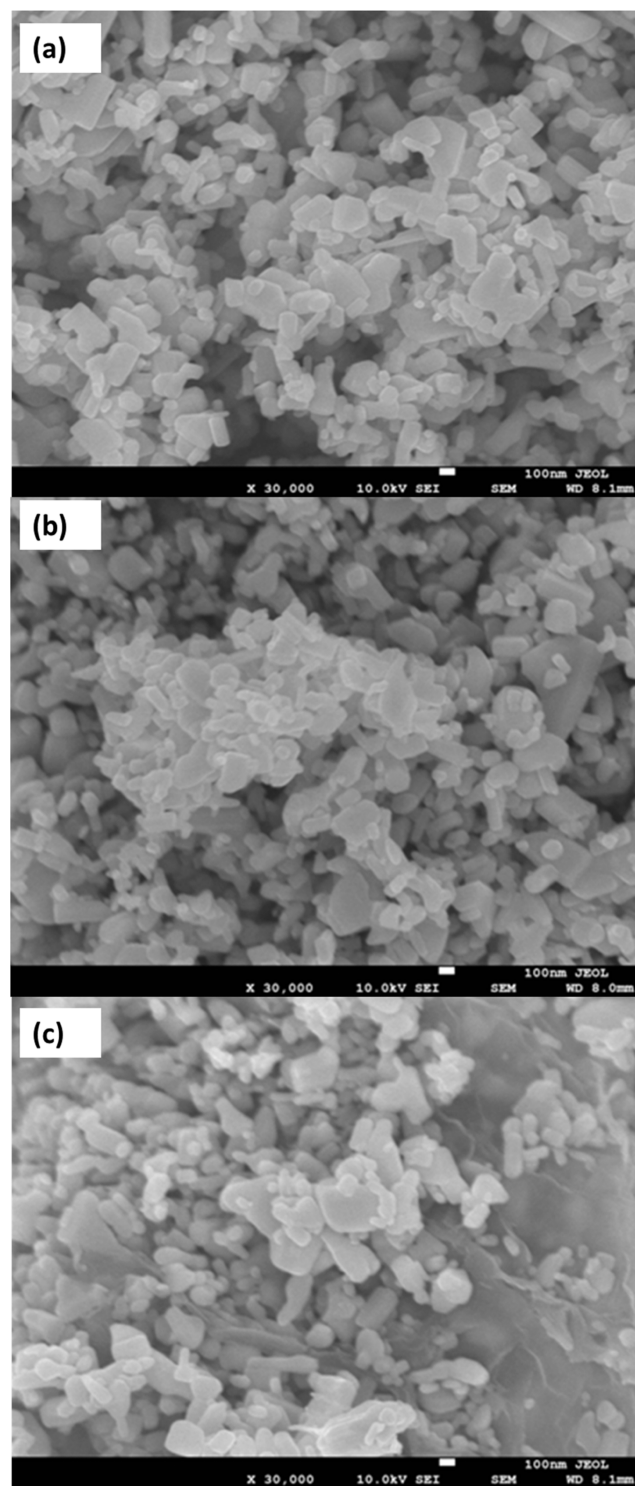

Figure 3. FESEM images of ZnO (a), g-C$_3$N$_4$/ZnO (b), and GO/g-C$_3$N$_4$/ZnO (c).

grain size of individual catalysts and their composites was determined using the Scherrer equation (eq 3)[43]

$$D = \frac{K\lambda}{\beta \cos \theta} \tag{3}$$

The average crystalline size (D) was calculated using the Scherrer equation, where β shows the full width at half-maximum of the diffraction peak patterns, while λ and K
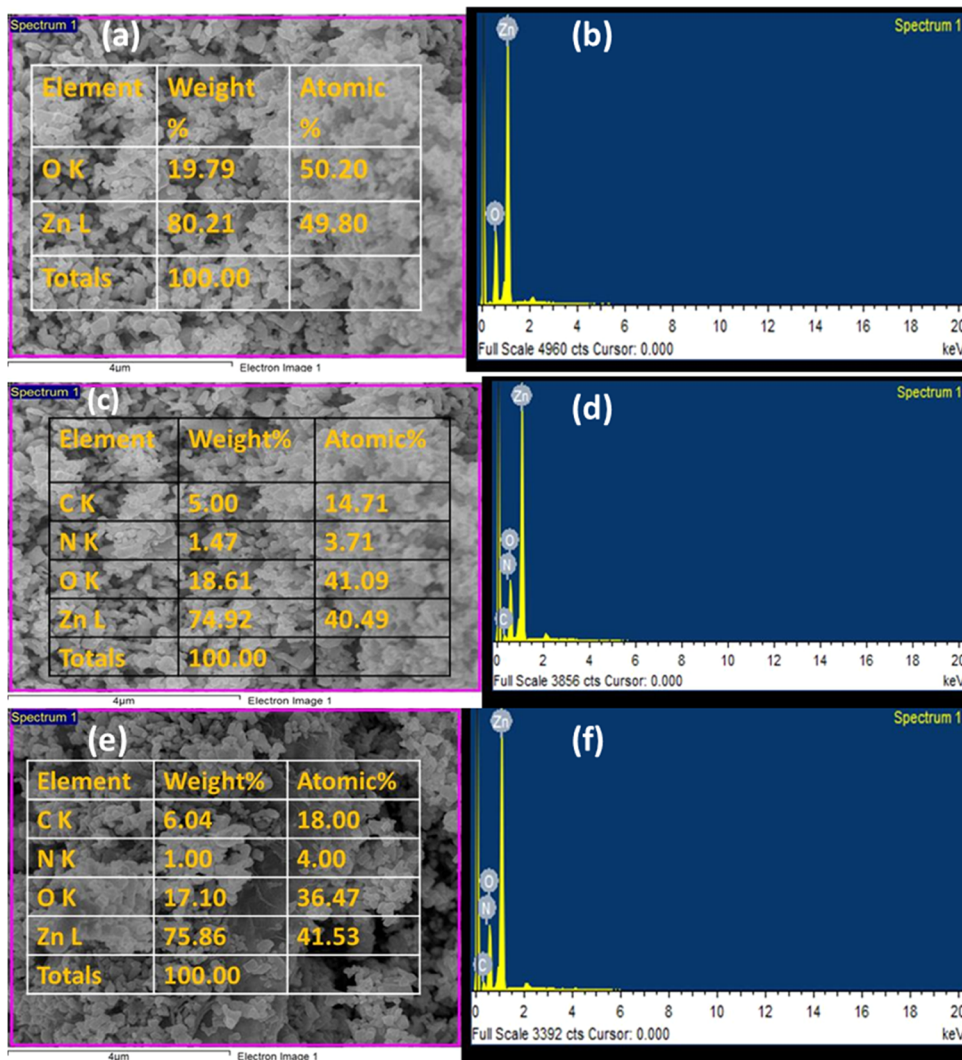
Figure 4. EDS compositional analyses and spectra of ZnO (a, b), g-C$_3$N$_4$/ZnO (c, d), and GO/g-C$_3$N$_4$/ZnO (e, f).

represent wavelength and constant, respectively. The average grain size of ZnO was determined to be 32.02 nm (Figure 2b).[44] Furthermore, the influence of ZnO lattice dislocation can be calculated based on the following relationship (eq 4):[37]

$$\delta = \frac{1}{D^2} \tag{4}$$

The results showed that the dislocation densities for ZnO, g-C$_3$N$_4$/ZnO, and GO/g-C3N4/ZnO were calculated to be 8.46 × 10^{-3}, 2.69 × 10^{-4}, and 2.96 × 10^{-4} nm, respectively. Changes in the dislocation density might influence the lattice strain of prepared ternary composite materials. Moreover, the lattice strain can be calculated using the following relationship (eq 5):[45]

$$\varepsilon = \frac{\beta \cos \theta}{4} \tag{5}$$

The estimated lattice strain values for ZnO, g-C$_3$N$_4$/ZnO, and GO/g-C$_3$N$_4$/ZnO were 1.03 × 10^{-3}, 1.41 × 10^{-3}, and 1.25 × 10^{-3} nm, respectively.[46]

3.3. SEM. The surface characterization of the sample was conducted by using field emission scanning electron microscopy (FESEM). The images analyzed by FESEM, which were taken at ×30k magnification, are presented in

Figure 3. Figure 3 revealed the rodlike structures within the composition of ZnO. In Figure 3b, a binary composite (g-C$_3$N$_4$/ZnO) is shown and showcasing ZnO nanorod structures alongside g-C$_3$N$_4$ particles. Figure 3c highlighted the GO sheets in addition to ZnO nanorods and also the unusually spherical-based g-C$_3$N$_4$ structures. The ZnO, which is the main material, maintained its rodlike distinct structure in both prepared nanocomposites, as illustrated in Figure 3a−c.[47]

3.4. EDS Spectra. All prepared samples were analyzed for elemental composition using energy-dispersive X-ray spectroscopy (EDS), and data are depicted in Figure 4. Figure 4a,b provided the elemental composition and EDS spectra of the newly prepared ZnO nanorods. Likewise, Figure 4c−f revealed the EDS outcomes for the binary (g-C$_3$N$_4$/ZnO) and ternary (GO/g-C$_3$N$_4$/ZnO) nanocomposites. The outcomes provided good evidence that the prepared nanocomposites exhibited exceptional purity and encompassing all of the necessary elements.[48]

The elemental mapping analysis of the ternary composite, GO/g-C$_3$N$_4$/ZnO, through EDS revealed a uniform distribution of constituent elements across the surface area. The compounded image in Figure S2a and individual elemental distributions in Figure S2b−e illustrate the even dispersion of carbon, nitrogen, oxygen, and zinc. This uniform distribution is
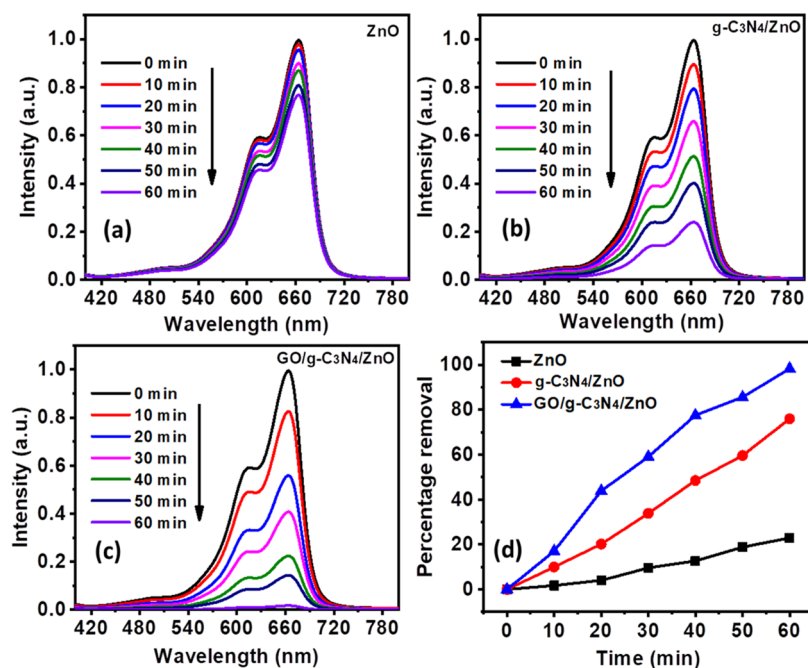
Figure 5. Photocatalytic degradation of ZnO (a), g-C₃N₄/ZnO (b), and GO/g-C₃N₄/ZnO (c), and percentage removal (d).
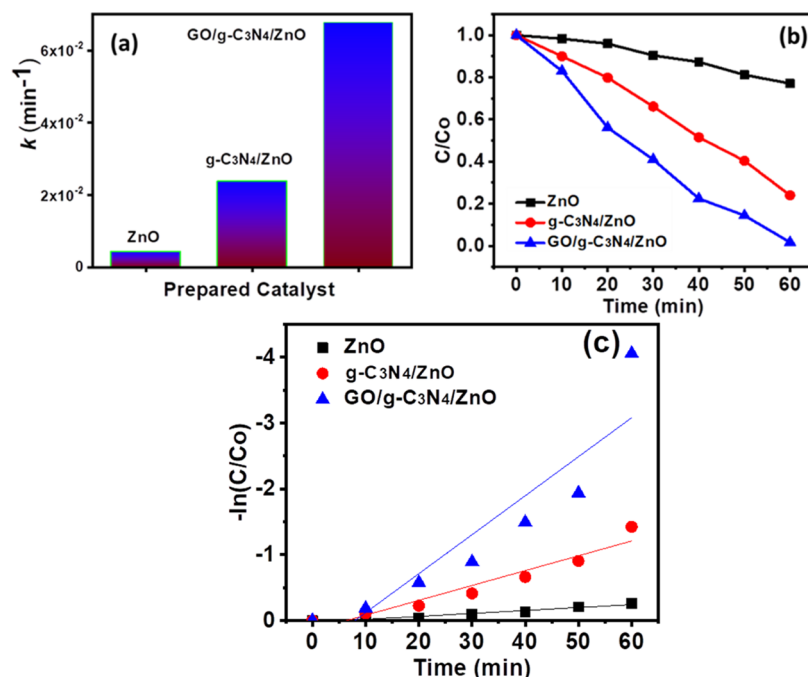

Figure 6. Degradation kinetics (a), apparent rate constant (b), and kinetics plot (c).

a noteworthy observation, emphasizing the homogeneity of the ternary composite.

3.5. Photocatalytic Degradation Study. The putative pollutant methylene blue dye was used to test the photocatalytic activity of ZnO, g-C₃N₄/ZnO, and GO/g-C₃N₄/ZnO in a batch reactor. A novel process involved mixing 50 mL of 200 mg/L dye and 0.1 g of the produced catalyst, agitating the mixture for 30 min in the dark. The outcomes were highly reproducible to within 5%. Figure 5a showed the results of the evaluation of ZnO's capacity to photocatalytically degrade MB. After 60 min, the absorbance peak reduced significantly for ZnO, g-C₃N₄/ZnO, and GO/g-C₃N₄/ZnO (Figure 5a−c).

ZnO displayed the MB degradation of 22.88%. ZnO has a lower rate of degradation, which is attributed to both its large band gap, as shown in Figure 5a, which restricted light absorption, and accelerated rate of electron−hole pair recombination during the process of conduction.[49] g-C₃N₄/ZnO demonstrated a 75.96% degradation of methylene blue; this increased MB degradation percentage was attributed to the narrower band gap,[50] which possibly enabled more visible light absorption, as shown in Figure 5b. In addition, it was discovered that combining ZnO, g-C₃N₄, and GO further improved MB degradation and leading to 90% degradation, as revealed by Figure 5c,d.
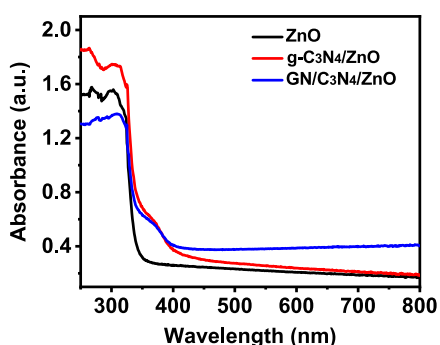
Figure 7. UV−vis spectra of prepared photocatalysts.

The rate constant and degradation kinetics were affected by adding different concentrations of prepared photocatalysts (Figure 6a−c). As we have seen in Figure 6b, when the photocatalyst was added, the degradation was increased with time.[51] When reaction time was reached at 60 min, the degradation of MB was maximum with a mixture containing GO/g-C_3N_4/ZnO. The rate constant for GO/g-C_3N_4/ZnO was 0.006 after 60 min, 0.003 for g-C_3N_4/ZnO, and 0.001 for ZnO photocatalyst. It was noted that the apparent rate constant was the maximum for GO/g-C_3N_4/ZnO after 60 min.

In conclusion, the proposed photocatalytic degradation mechanism of MB by GO/g-C_3N_4/ZnO demonstrated an enhanced performance under visible light irradiation. The absorption of photons by g-C_3N_4 initiated electron acceleration from the valence band to the conduction band. Following which, these electrons transfer to the conduction band of ZnO, while holes migrated toward the valence band of g-C_3N_4. This charge carrier separation reduces recombination. Moreover, changes in the work functions of GO and ZnO facilitated electron acceptance from ZnO, further minimizing charge recombination.[52] Consequently, the surplus charge carriers reached the surface of GO/g-C_3N_4/ZnO, where they plausibly engaged with water to generate hydroxyls and radicals.[53] The ensuing interaction with MB led to an amplified degradation of the dye, highlighting the efficiency of the photocatalytic process.

3.6. UV−Visible Spectroscopy. The photocatalytic degradability of ZnO, g-C_3N_4/ZnO, and GO/g-C_3N_4/ZnO composites was tested, and the results are shown in Figure 7. In Fenton's photocatalytic-like oxidation process, active species were produced through the separation, migration, and coupling of photogenerated charge carriers. One of these elements is the photocatalyst's capacity to absorb light, which impacts the Fenton-like oxidation process. To comprehend the absorption spectra property, the UV−vis absorption patterns of ZnO, g-C_3N_4/ZnO, and GO/g-C_3N_4/ZnO were investigated[37] (Figure 7). Only ultraviolet light having a wavelength of 400 nm or less can break up by pure ZnO nanorods. However, the GO/g-C_3N_4 caused the absorption zone to grow after loading in the visible range.[37] Additionally, the UV absorption edge of the photocatalyst exhibits a slight blue shift because of the size quantization effect brought on by the reduction in the ZnO nanorod size.

4. CONCLUSIONS

In conclusion, the addition of ZnO to g-C_3N_4/GO resulted in enhanced degradation of methylene blue through the photocatalytic processes during wastewater treatment. ZnO ex-hibited a 22.9% reduction in methylene blue concentration after 60 min of treatment. However, owing to its wide band gap that limits light absorption and its rapid electron−hole pair recombination rate during charge carrier conduction from the valence band to the conduction band, the catalytic activity of pure ZnO was somewhat diminished.

Specifically, the combination of ZnO and g-C_3N_4 led to an acceleration in methylene blue degradation, reaching 76.0%. Interestingly, the composite GO/g-C_3N_4/ZnO displayed the highest activity, with a notable 90% degradation of methylene blue achieved. In summary, the synthesized nanocomposite exhibited remarkable efficacy in removing methylene blue from polluted water. This prepared photocatalyst holds significant promise as an effective solution for eliminating toxic organic dyes from industrial wastewater discharges. It is therefore a valuable tool in addressing the environmental issue of tackling contaminated water discharges from industrial facilities.

■ ASSOCIATED CONTENT

ⓈI Supporting Information

The Supporting Information is available free of charge at https://pubs.acs.org/doi/10.1021/acsomega.3c10172.

XPS spectra and elemental analysis of prepared composite (PDF)

■ AUTHOR INFORMATION

Corresponding Authors

Muhammad Bilal Shakoor − *College of Earth & Environmental Sciences, University of the Punjab, Lahore 54590, Pakistan;* ⓞ orcid.org/0000-0002-3115-0234; Email: bilalshakoor88@gmail.com

Jean Wan Hong Yong − *Department of Biosystems and Technology, Swedish University of Agricultural Sciences, 23456 Alnarp, Sweden;* ⓞ orcid.org/0000-0003-3325-8254; Email: jean.yong@slu.se

Authors

Muhammad Hassan Shakoor − *Department of Chemistry, Riphah International University, Faisalabad 38000, Pakistan*

Asim Jilani − *Center of Nanotechnology, King Abdulaziz University, 21589 Jeddah, Saudi Arabia;* ⓞ orcid.org/0000-0001-5451-2050

Toheed Ahmed − *Department of Chemistry, Riphah International University, Faisalabad 38000, Pakistan*

Muhammad Rizwan − *Department of Environmental Sciences and Engineering, Government College University Faisalabad, Faisalabad 38000, Pakistan;* ⓞ orcid.org/0000-0002-3513-2041

Mohsin Raza Dustgeer − *Department of Environmental Sciences and Engineering, Government College University Faisalabad, Faisalabad 38000, Pakistan*

Javed Iqbal − *Center of Nanotechnology, King Abdulaziz University, 21589 Jeddah, Saudi Arabia*

Muhammad Zahid − *Department of Chemistry, University of Agriculture, Faisalabad 38000, Pakistan*

Complete contact information is available at:
https://pubs.acs.org/10.1021/acsomega.3c10172

Notes

The authors declare no competing financial interest.

■ REFERENCES

(1) Momina; Mohammad, S.; Suzylawati, I. Study of the adsorption/desorption of MB dye solution using bentonite adsorbent coating. *J. Water Process Eng.* **2020**, *34*, No. 101155.

(2) Kubra, K. T.; Salman, M. S.; Hasan, M. N. Enhanced toxic dye removal from wastewater using biodegradable polymeric natural adsorbent. *J. Mol. Liq.* **2021**, *328*, No. 115468.

(3) Taghizadeh, M. T.; Siyahi, V.; Ashassi-Sorkhabi, H.; Zarrini, G. ZnO, AgCl and AgCl/ZnO nanocomposites incorporated chitosan in the form of hydrogel beads for photocatalytic degradation of MB, *E. coli* and *S. aureus*. *Int. J. Biol. Macromol.* **2020**, *147*, 1018−1028.

(4) Zeebaree, A. Y. S.; Zeebaree, S. Y. S.; Rashid, R. F.; Zebari, O. I. H.; Albarwry, A. J. S.; Ali, A. F.; Zebari, A. Y. S. Sustainable engineering of plant-synthesized TiO2 nanocatalysts: Diagnosis, properties and their photocatalytic performance in removing of methylene blue dye from effluent. A review. *Curr. Res. Green Sustainable Chem.* **2022**, *5*, No. 100312. DOI: 10.1016/j.crgsc.2022.100312.

(5) Ramalingam, G.; Perumal, N.; Priya, A.; Rajendran, S. A review of graphene-based semiconductors for photocatalytic degradation of pollutants in wastewater. *Chemosphere* **2022**, *300*, No. 134391.

(6) Oyetade, J. A.; Machunda, R. L.; Hilonga, A. Photocatalytic degradation of azo dyes in textile wastewater by polyaniline composite catalyst-a review. *Sci. Afr.* **2022**, *17*, No. e01305. DOI: 10.1016/j.sciaf.2022.e01305.

(7) Jiang, X.; Yang, Z.; Li, W.; Liu, J.; Zhang, D.; Pu, X.; Cai, P. Thorny hydrangea-like $SnIn_4S_8/Mn_{0.3}Cd_{0.7}S$ as novel type-II heterojunction photocatalyst to enhance the efficient degradation of imidacloprid. *Appl. Surf. Sci.* **2023**, *617*, No. 156632.

(8) Norouzi, M.; Fazeli, A.; Tavakoli, O. Photocatalytic degradation of phenol under visible light using electrospun Ag/TiO_2 as a 2D nanopowder: Optimizing calcination temperature and promoter content. *Adv. Powder Technol.* **2022**, *33* (11), No. 103792.

(9) Pasini, S. M.; Valerio, A.; Yin, G.; Wang, J.; de Souza, S. M. G. U.; Hotza, D.; de Souza, A. A. U. An overview on nanostructured TiO_2−containing fibers for photocatalytic degradation of organic pollutants in wastewater treatment. *J. Water Process Eng.* **2021**, *40*, No. 101827.

(10) Durmus, Z.; Kurt, B. Z.; Durmus, A. Synthesis and characterization of graphene oxide/zinc oxide (GO/ZnO) nanocomposite and its utilization for photocatalytic degradation of basic fuchsin dye. *ChemistrySelect* **2019**, *4* (1), 271−278.

(11) Xie, M.; Gao, M.; Yun, Y.; Malmsten, M.; Rotello, V. M.; Zboril, R.; Akhavan, O.; Kraskouski, A.; Amalraj, J.; Cai, X. Antibacterial nanomaterials: mechanisms, impacts on antimicrobial resistance and design principles. *Angew. Chem., Int. Ed.* **2023**, *62* (17), No. e202217345. DOI: 10.1002/anie.202217345.

(12) Sun, Y.; Wang, T. *Application of Biochar, Adsorbent and Nanomaterials in Wastewater Treatment*; Multidisciplinary Digital Publishing Institute, 2023; Vol. *15*, p 1320.

(13) Zhang, D.; Zhang, D.; Wang, S.; Li, H.; Liu, J.; Pu, X.; Chen, P.; Qin, R.; Hu, H.; Cai, P. Synthesize magnetic $ZnFe_2O_4@ C/Cd_{0.9}Zn_{0.1}S$ catalysts with S-scheme heterojunction to achieve extraordinary hydrogen production efficiency. *J. Colloid Interface Sci.* **2024**, *657*, 672−683.

(14) Chen, Z.; Li, Y.; Cai, Y.; Wang, S.; Hu, B.; Li, B.; Ding, X.; Zhuang, L.; Wang, X. Application of covalent organic frameworks and metal−organic frameworks nanomaterials in organic/inorganic pollutants removal from solutions through sorption-catalysis strategies. *Carbon Res.* **2023**, *2* (1), 8.

(15) Eid, A. M.; Fouda, A.; Hassan, S. E.-D.; Hamza, M. F.; Alharbi, N. K.; Elkelish, A.; Alharthi, A.; Salem, W. M. Plant-based copper oxidenanoparticles; biosynthesis, characterization, antibacterial activity, tanning wastewater treatment, and heavy metals sorption. *Catalysts* **2023**, *13* (2), 348.

(16) Abuzeyad, O. H.; El-Khawaga, A. M.; Tantawy, H.; Elsayed, M. A. An evaluation of the improved catalytic performance of rGO/GO-hybrid-nanomaterials in photocatalytic degradation and antibacterial activity processes for wastewater treatment: A review. *J. Mol. Struct.* **2023**, *1288*, No. 135787. DOI: 10.1016/j.molstruc.2023.135787.

(17) Rahman, A.; Jennings, J. R.; Tan, A. L.; Khan, M. M. Molybdenum disulfide-based nanomaterials for visible-light-induced photocatalysis. *ACS Omega* **2022**, *7* (26), 22089−22110.

(18) Zhang, D.; Zhang, R.; Jiang, X.; Zhang, D.; Li, H.; Liu, J.; Pu, X.; Cai, P. A novel $SnIn_4 S_8/ZnFe_2 O_4$ S-scheme heterojunction with excellent magnetic properties and photocatalytic degradation activity for tetracycline. *Dalton Trans.* **2023**, *52* (41), 14956−14966.

(19) Sanakousar, F.; Vidyasagar, C.; Jiménez-Pérez, V.; Prakash, K. Recent progress on visible-light-driven metal and non-metal doped ZnO nanostructures for photocatalytic degradation of organic pollutants. *Mater. Sci. Semicond. Process.* **2022**, *140*, No. 106390.

(20) Wahid, F.; Zhao, X.-Q.; Cui, J.-X.; Wang, Y.-Y.; Wang, F.-P.; Jia, S.-R.; Zhong, C. Fabrication of bacterial cellulose with TiO_2-ZnO nanocomposites as a multifunctional membrane for water remediation. *J. Colloid Interface Sci.* **2022**, *620*, 1−13.

(21) Raghavendra, V. B.; Shankar, S.; Govindappa, M.; Pugazhendhi, A.; Sharma, M.; Nayaka, S. C. Green synthesis of zinc oxide nanoparticles (ZnO NPs) for effective degradation of dye, polyethylene and antibacterial performance in waste water treatment. *J. Inorg. Organomet. Polym. Mater.* **2022**, *32*, 614−630.

(22) Raha, S.; Ahmaruzzaman, M. ZnO nanostructured materials and their potential applications: progress, challenges and perspectives. *Nanoscale Adv.* **2022**, *4* (8), 1868−1925.

(23) Li, Z.; Wang, J.; Chen, H.; Wang, R.; Zhu, M. Synthesis of ZnO nanorod-decorated graphene oxide for application in dental resin composites. *ACS Biomater. Sci. Eng.* **2023**, *9* (5), 2706−2715.

(24) Abdullah, F.; Bakar, N. A.; Bakar, M. A. Current advancements on the fabrication, modification, and industrial application of zinc oxide as photocatalyst in the removal of organic and inorganic contaminants in aquatic systems. *J. Hazard. Mater.* **2022**, *424*, No. 127416.

(25) Tang, G.; Zhang, F.; Huo, P.; Zulfiqarc, S.; Xu, J.; Yan, Y.; Tang, H. Constructing novel visible-light-driven ternary photocatalyst of AgBr nanoparticles decorated 2D/2D heterojunction of g-C_3N_4/BiOBr nanosheets with remarkably enhanced photocatalytic activity for water-treatment. *Ceram. Int.* **2019**, *45* (15), 19197−19205.

(26) Sheng, W.; Li, W.; Tan, D.; Zhang, P.; Zhang, E.; Sheremet, E.; Schmidt, B. V.; Feng, X.; Rodriguez, R. D.; Jordan, R.; Amin, I. Polymer brushes on graphitic carbon nitride for patterning and as a SERS active sensing layer via incorporated nanoparticles. *ACS Appl. Mater. Interfaces* **2020**, *12* (8), 9797−9805.

(27) Umapathi, R.; Raju, C. V.; Ghoreishian, S. M.; Rani, G. M.; Kumar, K.; Oh, M.-H.; Park, J. P.; Huh, Y. S. Recent advances in the use of graphitic carbon nitride-based composites for the electrochemical detection of hazardous contaminants. *Coord. Chem. Rev.* **2022**, *470*, No. 214708.

(28) Chin, J. Y.; Ahmad, A. L.; Low, S. C. Graphitic carbon nitride photocatalyst for the degradation of oxytetracycline hydrochloride in water. *Mater. Chem. Phys.* **2023**, *301*, No. 127626.

(29) Jiříčková, A.; Jankovský, O.; Sofer, Z.; Sedmidubský, D. Synthesis and applications of graphene oxide. *Materials* **2022**, *15* (3), 920.

(30) Velusamy, S.; Roy, A.; Sundaram, S.; Kumar Mallick, T. A review on heavy metal ions and containing dyes removal through graphene oxide-based adsorption strategies for textile wastewater treatment. *Chem. Rec.* **2021**, *21* (7), 1570−1610.

(31) Joshi, N. C.; Gururani, P. Advances of graphene oxide based nanocomposite materials in the treatment of wastewater containing heavy metal ions and dyes. *Curr. Res. Green Sustainable Chem.* **2022**, *5*, No. 100306.

(32) Kurniawan, T. A.; Mengting, Z.; Fu, D.; Yeap, S. K.; Othman, M. H. D.; Avtar, R.; Ouyang, T. Functionalizing TiO_2 with graphene

oxide for enhancing photocatalytic degradation of methylene blue (MB) in contaminated wastewater. *J. Environ. Manage.* **2020**, *270*, No. 110871.

(33) Marjani, A.; Nakhjiri, A. T.; Adimi, M.; Jirandehi, H. F.; Shirazian, S. Effect of graphene oxide on modifying polyethersulfone membrane performance and its application in wastewater treatment. *Sci. Rep.* **2020**, *10* (1), No. 2049.

(34) Marcano, D. C.; Kosynkin, D. V.; Berlin, J. M.; Sinitskii, A.; Sun, Z.; Slesarev, A.; Alemany, L. B.; Lu, W.; Tour, J. M. Improved synthesis of graphene oxide. *ACS Nano* **2010**, *4* (8), 4806−4814.

(35) Kumar, S. S.; Venkateswarlu, P.; Rao, V. R.; Rao, G. N. Synthesis, characterization and optical properties of zinc oxide nanoparticles. *Int. Nano Lett.* **2013**, *3*, 30.

(36) Zhu, J.; Xiao, P.; Li, H.; Carabineiro, S. A. Graphitic carbon nitride: synthesis, properties, and applications in catalysis. *ACS Appl. Mater. Interfaces* **2014**, *6* (19), 16449−16465.

(37) Saeed, U.; Jilani, A.; Iqbal, J.; Al-Turaif, H. Reduced graphene oxide-assisted graphitic carbon nitride@ ZnO rods for enhanced physical and photocatalytic degradation. *Inorg. Chem. Commun.* **2022**, *142*, No. 109623.

(38) Zeng, G.; He, Z.; Wan, T.; Wang, T.; Yang, Z.; Liu, Y.; Lin, Q.; Wang, Y.; Sengupta, A.; Pu, S. A self-cleaning photocatalytic composite membrane based on g-C₃N₄@ MXene nanosheets for the removal of dyes and antibiotics from wastewater. *Sep. Purif. Technol.* **2022**, *292*, No. 121037.

(39) Liao, G.; Yao, W. Facile synthesis of porous isotype heterojunction g-C₃N₄ for enhanced photocatalytic degradation of RhB under visible light. *Diamond Relat. Mater.* **2022**, *128*, No. 109227.

(40) Wang, S.; Li, Y.; Wang, X.; Zi, G.; Zhou, C.; Liu, B.; Liu, G.; Wang, L.; Huang, W. One-step supramolecular preorganization constructed crinkly graphitic carbon nitride nanosheets with enhanced photocatalytic activity. *J. Mater. Sci. Technol.* **2022**, *104*, 155−162.

(41) Moulder, J. F.; Chastain, J. *Handbook of X-ray Photoelectron Spectroscopy: A Reference Book of Standard Spectra for Identification and Interpretation of XPS Data*; Physical Electronics Division, Perkin-Elmer Corporation, 1992.

(42) Wang, C.; Wu, D.; Wang, P.; Ao, Y.; Hou, J.; Qian, J. Effect of oxygen vacancy on enhanced photocatalytic activity of reduced ZnO nanorod arrays. *Appl. Surf. Sci.* **2015**, *325*, 112−116.

(43) Danish, M.; Athar, M. S.; Ahmad, I.; Warshagha, M. Z.; Rasool, Z.; Muneer, M. Highly efficient and stable Fe₂O₃/g-C₃N₄/GO nanocomposite with Z-scheme electron transfer pathway: Role of photocatalytic activity and adsorption isotherm of organic pollutants in wastewater. *Appl. Surf. Sci.* **2022**, *604*, No. 154604.

(44) Wang, L.; Chen, T. Simultaneously enhancing strength and toughness of graphene oxide reinforced ZK60 magnesium matrix composites through powder thixoforming. *Composites, Part A* **2022**, *161*, No. 107097.

(45) Zakria, H. S.; Othman, M. H. D.; Kamaludin, R.; Jilani, A.; Omar, M. F.; Ayub, M.; Saidin, M. A. R.; Kurniawan, T. A.; Hashim, N.; Yahaya, N. K. E.; et al. Removal of bisphenol A from synthetic and treated sewage wastewater using magnetron sputtered CuxO/PVDF thin film photocatalytic hollow fiber membrane. *J. Water Process Eng.* **2023**, *51*, No. 103425.

(46) Sun, X.; Shi, Y.; Lu, J.; Shi, W.; Guo, F. Template-free self-assembly of three-dimensional porous graphitic carbon nitride nanovesicles with size-dependent photocatalytic activity for hydrogen evolution. *Appl. Surf. Sci.* **2022**, *606*, No. 154841.

(47) Li, S.; Hasan, N.; Ma, H.; Li, O. L.; Lee, B.; Jia, Y.; Liu, C. Significantly enhanced photocatalytic activity by surface acid corrosion treatment and Au nanoparticles decoration on the surface of SnFe₂O₄ nano-octahedron. *Sep. Purif. Technol.* **2022**, *299*, No. 121650.

(48) BinSabt, M.; Sagar, V.; Singh, J.; Rawat, M.; Shaban, M. Green synthesis of CS-TiO₂ NPs for efficient photocatalytic degradation of methylene blue dye. *Polymers* **2022**, *14* (13), 2677.

(49) Antonopoulou, M.; Bika, P.; Papailias, I.; Zervou, S.-K.; Vrettou, A.; Efthimiou, I.; Mitrikas, G.; Ioannidis, N.; Trapalis, C.; Dallas, P.; et al. Photocatalytic degradation of organic micropollutants under UV-A and visible light irradiation by exfoliated g-C₃N₄ catalysts. *Sci. Total Environ.* **2023**, *892*, No. 164218.

(50) Ismael, M. Environmental remediation and sustainable energy generation via photocatalytic technology using rare earth metals modified g-C₃N₄: A review. *J. Alloys Compd.* **2023**, *931*, No. 167469, DOI: 10.1016/j.jallcom.2022.167469.

(51) Verma, M. L.; Sukriti; Dhanya, B.; Saini, R.; Das, A.; Varma, R. S. Synthesis and application of graphene-based sensors in biology: a review. *Environ. Chem. Lett.* **2022**, *20* (3), 2189−2212.

(52) Negash, A.; Mohammed, S.; Weldekirstos, H. D.; Ambaye, A. D.; Gashu, M. Enhanced photocatalytic degradation of methylene blue dye using eco-friendly synthesized rGO@ZnO nanocomposites. *Sci. Rep.* **2023**, *13* (1), No. 22234.

(53) Shen, J.-H.; Chiang, T.-H.; Tsai, C.-K.; Jiang, Z.-W.; Horng, J.-J. Mechanistic insights into hydroxyl radical formation of Cu-doped ZnO/g-C₃N₄ composite photocatalysis for enhanced degradation of ciprofloxacin under visible light: Efficiency, kinetics, products identification and toxicity evaluation. *J. Environ. Chem. Eng.* **2022**, *10* (2), No. 107352.